

PAPER

An interpretation and guide to single-pass beam shaping methods using SLMs and DMDs

To cite this article: Alexander B Stilgoe *et al* 2016 *J. Opt.* **18** 065609

View the [article online](#) for updates and enhancements.

You may also like

- [Broadband structured light using digital micro-mirror devices \(DMDs\): a tutorial](#)
Leerin Perumal and Andrew Forbes
- [CT scanner-specific organ dose coefficients generated by Monte Carlo calculation for the ICRP adult male and female reference computational phantoms](#)
Jan TM Jansen, Paul C Shrimpton and Sue Edyvean
- [Wave characterisation and aberration correction using hybrid direct search](#)
Alexander B Stilgoe and Halina Rubinsztein-Dunlop

An interpretation and guide to single-pass beam shaping methods using SLMs and DMDs

Alexander B Stilgoe¹, Anatolii V Kashchuk¹, Daryl Preece² and Halina Rubinsztein-Dunlop¹

¹ School of Mathematics and Physics, The University of Queensland, The University of Queensland, St. Lucia, QLD, 4072, Australia

² Department of NanoEngineering, University of California, San Diego, 9500 Gilman Drive La Jolla, California 92093, USA

E-mail: a.stilgoe@uq.edu.au

Received 25 February 2016, revised 17 March 2016

Accepted for publication 30 March 2016

Published 11 May 2016



Abstract

Exquisite manipulations of light can be performed with devices such as spatial light modulators (SLMs) and digital micromirror devices (DMDs). These devices can be used to simulate transverse paraxial beam wavefunction eigenstates such as the Hermite–Laguerre–Gaussian mode families. We investigate several beam shaping methods in terms of the wavefunctions of scattered light. Our analysis of the efficiency, behaviour and limitations of beam shaping methods is applied to both theory and experiment. The deviation from the ideal output from a valid beam shaping method is shown to be due to experimental factors which are not necessarily being accounted for. Incident beam mode shape, aberration, and the amplitude/phase transfer functions of the DMD and SLM impact the distribution of scattered light and hence the effectiveness and efficiency of a beam shaping method. Correcting for these particular details of the optical system accounts for all differences in efficiency and mode fidelity between experiment and theory. We explicitly show the impact of experimental parameter variations so that these problems may be diagnosed and corrected in an experimental beam shaping apparatus. We show that several beam shaping methods can be used for the production of beam modes in a single pass and the choice is based on the particular experimental conditions.

Keywords: beam profile, wave propagation, transmission, optical trapping, beam shaping, aberration, scattering

(Some figures may appear in colour only in the online journal)

1. Introduction

The production of high-fidelity beam modes is of interest in a diverse range of sub-fields of physics and engineering such as optics [1], quantum mechanics [2], communication [3], 3D printing [4], and optical manipulation [5]. Our work focuses on the applications of beam shaping involving spatial light modulators (SLMs) and digital micromirror devices (DMDs) as these are quite commonly used in electronics and optics laboratories. The problem with these devices is that neither device in a single pass can produce the scattered light with extreme precision or fidelity except in simple cases where

precise control of amplitude and phase is not needed. There has long been need to solve these difficulties and the field of beam shaping is mature and a large number of methods can be found in the literature [6–16] (though not exhaustively listed here). Beam shaping methods can involve single scattering or multiple scattering passes and have greatly differing efficiencies and fidelities. Here we build up a formalism using wavefunctions and the analysis of wavefunctions so that phase modulated and amplitude modulated shaping methods can be consistently compared.

We concentrate our attention on the production of high-order Laguerre–Gaussian beams using the beam shaping

methods we outline. We present a broad comparison of the operation of SLMs and DMDs when producing these beams. We show how the correct application of the methods achieve high performance realisation in an experimental system. Considering the single-pass methods as a family of methods in a wavefunction picture leads (as demonstrated in the next section) to the conclusion that only the capabilities of the device determines the efficiency and fidelity of resulting modes and not the particulars of a valid method. We show this principle both in experiment and in computer simulation.

2. Wavefunctions, dither, and diffraction efficiency

In the regime where the propagation of light is adequately described by the paraxial wave equation we can define a transverse wavefunction at any plane,

$$\psi(x, y) = A(x, y) \exp i\phi(x, y), \quad (1)$$

where the wavefunction is a function of the transverse position x, y and A and ϕ are respectively the amplitude and phase (argument³) of the wavefunction. The propagation of the wavefunction is modified by devices such as the SLM and DMD by changing the strength and argument of modes. Often the devices used for mode conversion have limitations in both the amount of, and resolution of, phase and amplitude modulation of the incident light. Consequently, their ability to accurately produce the desired mode is compromised by the generation of additional modes which interfere as the wave propagates. Corrections to the phase and amplitude functions need to be applied and filtering needs to be performed to produce the desired mode. For a device with discrete phase and/or amplitude control a process called *dithering* [17] is used to approximate the idealised signal in one of these planes and filtering is employed in the other to allow the target wavefunction to be transmitted.

Figure 1(a) shows the ideal wavefunction in the device plane. Figure 1(b) shows a wavefunction with amplitude restricted to a dithered amplitude of 0 or 1 with fixed (but ideal) phase. Figure 1(c) shows a wavefunction with amplitude restricted to amplitude 1 and dithered phase of 0 or π . In the target region of the imaging plane shown in figure 1(d) we see that there is excellent agreement between the ideal, amplitude modulated and phase modulated signals (they are on top of each other). Outside this region, however, the signals can and do substantially vary. The more limitations a device has, the more the conversion efficiency reduces. The diffraction efficiency as we define it (amount of light propagating in the target mode) of a discrete device can be calculated using the overlap between the amplitude normalised target output state and the amplitude normalised state

produced by the device

$$\eta = \left| \frac{\sum_{n,m} U_{mn}^* \psi_{mn}}{\sqrt{(\sum_{n,m} U_{mn}^* U_{mn})(\sum_{n,m} \psi_{mn}^* \psi_{mn})}} \right|, \quad (2)$$

where U_{mn} is the modulated mode amplitude scattered by the device as a function of device pixel/element index and ψ_{mn} is the wavefunction at each pixel with complex conjugates denoted with a star, \star . If we are successful in choosing the correct scalar pattern for the mode shaping device we will have changed the mode amplitudes of the scattered light as a function of angle, but not the total available light. A complicated distribution of light is produced with other (non-desired) mode amplitudes elsewhere in space.

Most methods of both amplitude and phase modulations implicitly use dithering of the wavefunction as the physical operating principle as it is the only way devices with constraints can approximate these wavefunctions. The mathematics used to construct mode shaping methods doesn't require explicit knowledge about the devices used to produce the modes. Therefore, many of the methods can be misused and produce modes of poor quality. Using the wavefunction picture of the beam shaping method is a broader foundation as it is strongly connected to the interpretation of the result of beam shaping. The analysis of the mode altering device needs to be explicitly defined in this picture and therefore the method most compatible with the device is considered. The optimisation is only performed for a small region of the image plane, there is no necessary requirement of uniqueness of the pattern used for mode shaping with a device except to particular sets of patterns as restricted by its ability to modulate the phase and amplitude of the incident wavefunction. The mode shaping we wish to perform is spatial in nature. We are therefore limited by the number of spatial states available on the device. The result in this section demonstrates that given sufficiently large numbers of spatial states on the device we can produce any locally defined wavefunction with as little as two phase or amplitude state control and the appropriate dither.

3. Experimental design

We performed an experimental investigation to verify our theoretical models. The apparatus consists of Ytterbium-doped fibre laser operating at 1070 nm (YLM-5-LP, IPG Photonics), transfer optics, SLM (P512-1064, Meadowlark Optics, Inc.)/DMD (DLP4500VIS, Texas Instruments) and a digital camera (Lw115, Lumenera Corporation) to image the resulting beam modes. For our experiments we chose a Laguerre–Gaussian target mode with radial index, $p = 1$, and azimuthal index, $l = 3$. This apparatus is shown in figure 2.

Finding the correspondence between the pixel grey level (voltage) on the SLM and optical phase level can be challenging but necessary to ensure that some of the beam shaping methods accurately produce the desired beam modes (an example for this is demonstrated in the results section).

³ $\arg x \equiv -i \ln \frac{x}{|x|}$.

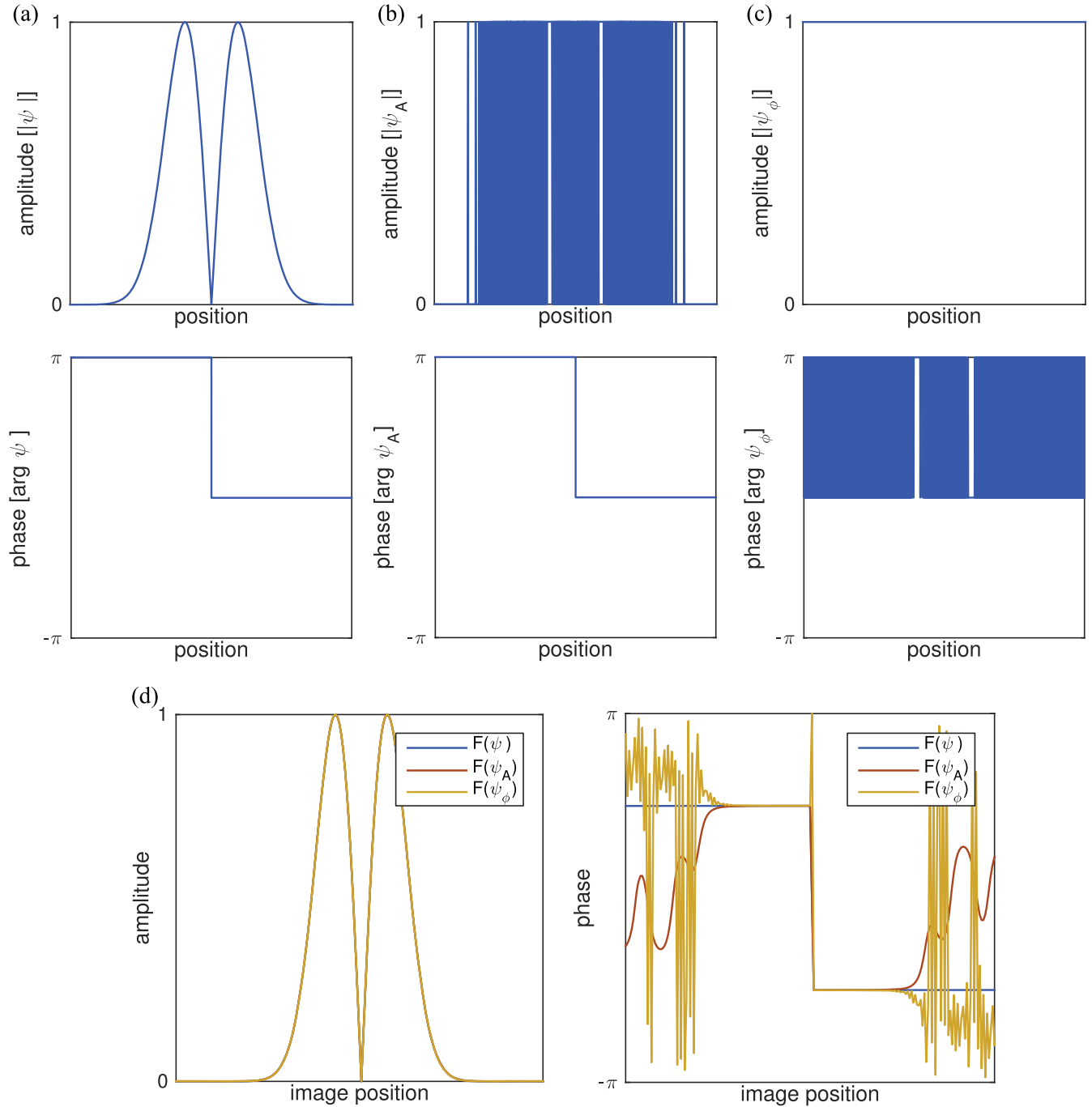


Figure 1. The ideal wavefunction and two locally optimised wavefunctions. The amplitude and argument of the (a) ideal wavefunction, (b) amplitude modulation approximated wavefunction flips between the null state and 1 are at spatial frequencies greater than the plot resolution so appear as a solid colour. (c) Phase modulation approximated wavefunction has flips between 0 and π at frequencies higher than the plot resolution and also appear as solid colour with exception at where the peak amplitude would be, here it has the phase of the ideal wavefunction. (d) The resulting amplitude and phase of mode amplitudes around a region local to the maximum amplitude of the ideal wavefunction in the image plane.

Usually, the characterisation of an SLM is performed with interferometry which can also elucidate other device properties such as cross-talk due to field effects across adjacent device elements [18–20]. Instead of performing a full characterisation of the SLM it was sufficient for our purposes to find an approximation of the conversion of grey level and phase by finding the maximum diffraction efficiency for a linear function and tuning the curvature of the function to

produce a large diffraction efficiency. The function displayed on the SLM was defined by

$$v_{mn}(s, g) = \text{mod}\left(s + \frac{g}{255} \text{mod}_{255} g_n(n - 128)\right), \quad (3)$$

where v_{mn} is the voltage level of the SLM for each pixel (index: m, n) in terms of colour offset $\in [0, 255]$, s is the grey level offset, and g is the gradient of the wedge function. The

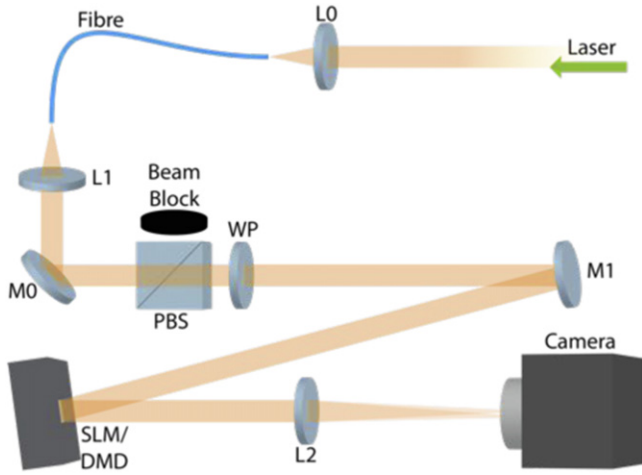


Figure 2. The experimental apparatus used to image beam modes. The apparatus consists of a NIR laser at 1070 nm passing through a polarisation maintaining mode cleaner, (lenses L0, L1 and polarisation maintaining single mode fibre). The quality of the polarisation can be inferred from a difference signal at the beam block. A half-waveplate, WP, can be used to optimise the polarisation of the laser for optimal scattering from the SLM/DMD. A lens, L2, focuses the light scattered off the diffractive optical element onto a CCD camera.

result of scanning offset and linear lookup for the SLM in our experimental system is shown in figure 3. The best linear approximation to phase level look-up is found from the parameters, offset and pixel grey level (voltage) which produce the maximum diffracted light.

As aberrations are always present in optical systems a phase/amplitude correction method was employed to construct a phase and amplitude correction mask for the laser wavelength we are using [21]. In a paraxial system, the phase correlations between different sections of both SLMs and DMDs are directly observable through the analysis of an interferogram recorded by the camera. Analysis was performed by taking regions of interest surrounding the interference pattern and running a Fourier transform of the time series for each pixel. This was reformed into a map of phase and amplitude for each pixel. A 2D Fourier transform was used to extract the phase (argument, P_{mn}) and amplitude (A_{mn}) of each pattern transmitted through the device. Once the wavefront distortions have been found they can be effectively undone by applying the reverse operations to the distortion the device applied. Removing this distortion has the effect of transforming the target wave function amplitudes into more idealised counterparts. This is achieved in phase by introducing the conjugate phase $-P_{mn}$ and in amplitude by applying the inverse amplitude $1/A_{mn}$ when calculating the scattering function displayed on the device. As we are limited to either amplitude or phase manipulations the phase and amplitude corrections must form part of any wavefunction dithering scheme to produce the highest mode fidelity. The application of these phase and amplitude corrections are method specific and will be discussed in more detail in the single-pass methods section.

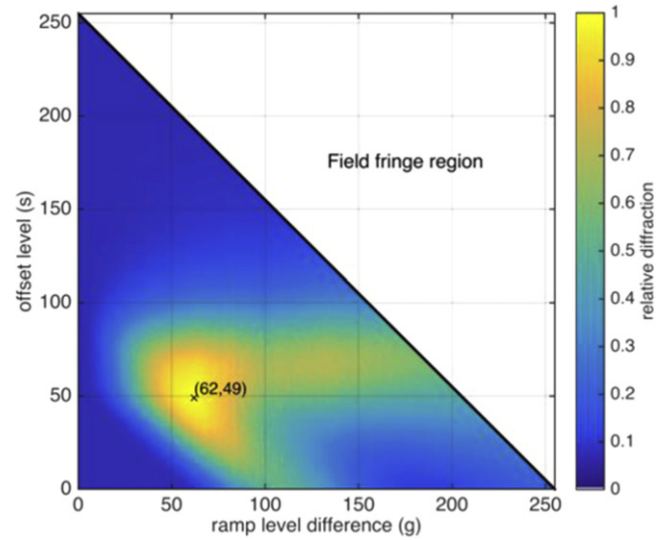


Figure 3. Scanning over the offset ramp function defined by equation (3). Due to field effects, scanning over ranges which wrap around from high levels to low levels will result in scenarios where phase patterns result in highly variable scattered light fields it was therefore not sampled. The maximum diffraction efficiency for the look-up ramp is demarked with a \times .

The dithering pattern used for both the SLM and DMD incorporated both phase and amplitude corrections as part of the resulting pattern. The resulting dithered phase pattern was displayed on the SLM using standard video output. The model of DMD used in these experiments cannot be reliably used to accurately produce beam modes in its standard video display mode due to the pixel interpolation scheme used by the firmware. Instead the images were displayed from internal flash memory. In this operational mode it was possible to configure the output to prevent the interpolation scheme.

The mode produced by the SLM and DMD using our experimentally determined parameters is

$$U_{mn} = H_{mn}A_{mn} \exp i(P_{mn} + \phi_{mn}), \quad (4)$$

where H_{mn} is the switching function of the DMD, ϕ_{mn} is the phase produced by the SLM and A_{mn} and P_{mn} is the amplitude and phase at the device plane for the incident radiation. For SLMs, $H_{mn} = 1$, and for DMDs, $\phi_{mn} = 0$.

A high-dynamic range algorithm was used in the image capture process [22] so that low intensity detail such as random noise floors could be resolved and to linearise the pixel response at high intensities.

4. Single-pass methods

Single-pass methods enable beam shaping through the use of a spatial band-pass filter by dithering of a wavefunction with a distinct signal. Phase and amplitude filtering of light for the control of systems can find its roots with some early signal processing of measured light, as an example, Kozma and Kelly (1965) [6]. Work on signal processing using phase plates by Kirk *et al* [7] convincingly demonstrated that one can produce a desired mode with both well defined amplitude

and phase in a localised region of space to high fidelity using a static pattern limited to information on phase shifts only. The same was shown for ‘amplitude’ only devices by Brown and Lohmann a few years earlier [23] where manipulations are subject to the exact same wave diffraction physics though restricted to functions which are mirrored around the reflection mode⁴. In both cases bandpass filtering (via spatial filter) can be applied to allow only the desired phase and amplitude information to be transmitted. Let us consider what DMDs and SLMs do to the incident wavefunction. Our goal in mode shaping is to manipulate both the probability amplitudes of a wavefunction and its argument for filtering in some plane. An SLM cannot affect the amplitude of the waveform at the device, but it can modify the phase noise. It is well known that phase noise changes the amplitude of a wave as it propagates. Thus phase noise modulation must be the solution for mode shaping with SLMs. DMDs have direct control of the amplitude of the waveform, but not the phase, therefore amplitude noise must be added instead. To first approximation, the solution to our problem for both devices needs the introduction of diffraction (dithering) functions which are distinct from the wavefunction we wish to transmit through the optical system. The choice of these diffraction functions is theoretically arbitrary, but strictly limited by the capabilities of the device: e.g. finite element number and typically 256 phase/amplitude levels on a SLM (over 2π) and single amplitude/phase level on a binary DMD. One of the ways beam shaping could be achieved is to use multi-order diffraction as it is possible to choose a grating period large enough to stop significant interference between the multiple orders. The first diffraction order is always determined by the period over which a modulo 2π shift is achieved and the efficiency in the n th order is determined by the overlap of the n th order function and the discontinuous function. Thus on a device capable of phase control, controlling the degree of discontinuity manipulates the amount of amplitude in each order. The pitch, c , of the phase function, $\arg D_{mn}$, producing multiple-order diffraction amplitudes obey the equation

$$\eta(c) = \frac{1}{N} \sum_{n,m} \exp i(o - c)\arg D_{mn}, \quad (5)$$

where $\eta(c)$ is the peak mode amplitude, N is the number of elements and o is the order of diffraction. For periodic functions in the continuum this sum results in

$$\eta(c) = \text{sinc}(o - c), \quad (6)$$

which means linear changes in pitch of the pattern result in sinc function dependence of amplitudes. To linearise the diffracted amplitude we need to find the inverse of this function, which is undefined over domains which do not pass the horizontal line test. Let us consider only the first order $o = 1$ and $c \in [0, 1]$, the inverse function is:

$$c = 1 - \text{sinc}^{-1}(\eta(c)), \quad (7)$$

⁴ The background theory was derived by Abbe for the investigation of the diffraction in microscopes [24].

which is the result of Kirk *et al* [7] found through different means. Provided that the dithering signal has frequent phase discontinuities almost any shift of a mode can be produced from devices capable of phase gradient shifts of light. This relation is not limited to uniform phase gradients, almost any arbitrary function can be used provided it contains enough phase discontinuities. Say we are using an SLM effectively producing the modes:

$$U_{mn} = X_{mn} \exp i(\arg \psi_{mn} + c_{mn} \arg D_{mn} - P_{mn}), \quad (8)$$

where ψ_{mn} is the target wavefunction, c_{mn} is the weighting of dither function D_{mn} at each point of the device, X_{mn} is the measured amplitude and phase aberrations with phase correction $-P_{mn}$. For the example outlined here c_{mn} takes the values

$$c_{mn} = 1 - \text{sinc}^{-1} |\psi_{mn}^{(N)}/A_{mn}|, \quad (9)$$

where $\psi_{mn}^{(N)}$ is the amplitude normalised target wavefunction and A_{mn} is the normalised light amplitude on each element of the device. Normalisation in this way ensures that the diffracted power is optimised in the target mode and takes account of the measured amplitude distortions. In cases where the relative incident amplitude drops below the relative amplitude of the target wavefunction the amount of light deflected can substantially reduce if the target wavefunction is precisely required. The output may be approximately produced by setting values outside $|\psi_{mn}^{(N)}/A_{mn}| \leq 1$ to 1. If we instead use the argument, $\arg D_{mn} = (-1)^n (-1)^m \pi/2$, we obtain a special case [14]. The diffraction efficiency for this pattern (appendix) is

$$\eta(c) = \cos(1 - c) \frac{\pi}{2}, \quad (10)$$

which has the inverse:

$$c = 1 - \frac{2}{\pi} \cos^{-1}(\eta(c)). \quad (11)$$

Figure 4 shows the result of using the two methods defined here. To remove the reflection mode from the SLM experiments the patterns displayed incorporated a large wedge grating function which was applied to the beam shaping hologram to move the resulting pattern to another part in space. Figures 4(a)–(c) are the phase patterns used to simulate the far-field and figures 4(d)–(f) correspond to the mode amplitudes in the conjugate plane. (a) Uses the argument of the conjugate of the wavefunction and blazing function as the phase dithering pattern, (b) uses an alias pattern to dither, (c) uses white noise to dither. Out of the three corresponding mode amplitudes the random noise pattern has the most interference as there are components of the dithering pattern which diffract to the same location as the desired mode amplitudes. Experimental realisations of these patterns are also shown in figures 4(g)–(i). As the colour scheme for each plot uses the same scale we can observe that each method shows the same efficiency and clarity (fidelity) in mode production though without mode tomography this is not definitive. The differences only appear in the surrounding signals resulting from the introduction of dithering and a

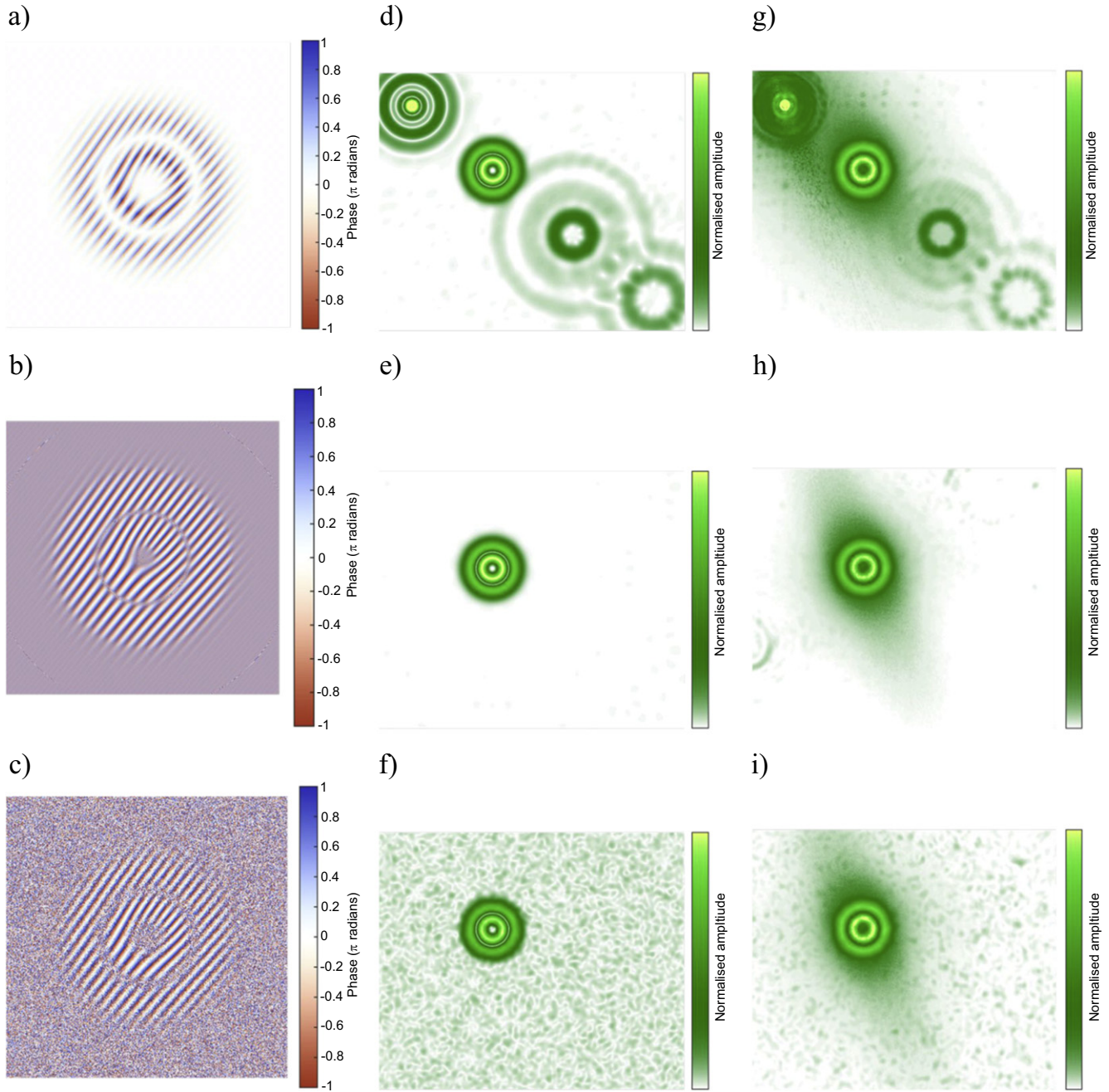


Figure 4. The phase-only holograms (a)–(c) and the diffracted pattern in the conjugate imaging plane for the zero-th and first three orders both in simulation (d)–(f) and experiment (g)–(i). Holograms for a stationary transverse state of the paraxial wave equation where (a) $D_{mn} = \exp -i(k_x x_m + k_y y_n + \arg \psi_{mn})$ the conjugate of the target wavefunction and the phase gradient applied to it, (b) $D_{mn} = \exp i(-1)^{(n+m)}\pi/2$ the alias signal, (c) $D_{mn} = \exp i2\pi\nu_{mn}$ a white distribution of noise (ν).

small amplitude halo resulting from the point spread function. Local to the target amplitudes there is a high degree of correspondence between each implementation.

An amplitude modulator operates under similar principles to phase modulators. Unlike the phase only modulator the probability (amplitude) distribution function can be modified at the device plane. However, as it only can have one phase it must split power evenly between positive and negative diffraction orders with significant zero order (reflection/transmission) mode amplitudes. Abbe’s

diffraction theory of microscopes informs us that the amplitude of a particular diffraction order is controlled in a binary amplitude grating by the ratio of segment lengths of on and off states [24]. To illustrate this effect, consider:

$$U_{mn} = \begin{cases} 1 & \cos \arg D_{mn} > 0 \\ 0 & \text{otherwise,} \end{cases} \quad (12)$$

where necessarily this has a spectra of diffraction orders [24] mirrored around the reflection mode and a loss channel.

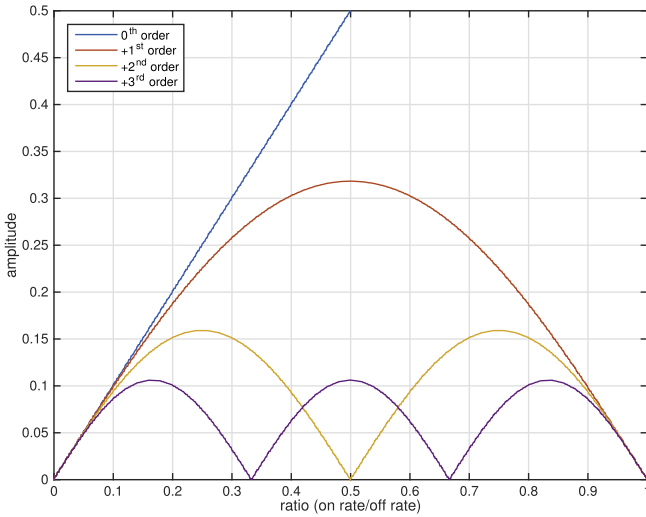


Figure 5. Amplitude in the 0th and first three diffraction orders for a uniformly spaced binary grating with on/off rate. The first order has sine dependence as predicted by diffraction theory. The 0th order is proportional to the reduction of amplitude in the loss channel as each element is switched on.

Depending on the required temporal or spatial stability or accuracy dithering may be achieved by either rapid switching of the device elements or the introduction of some other poorly overlapping function (as before). The amplitude in the first three +ve orders as a function of on/off rates of a simple grating of fixed periodicity is shown in figure 5. On a real device the total amount of light reflected will be scaled by the reflection efficiency. Variations of amplitude as a function of element location can also be accounted for locally by changing the surrounding dither as shown in equation (14).

Picking the first order we observe sinusoidal dependence of amplitude on the on/off rate. Somewhat predictably we get the largest diffraction efficiency when equal number of elements are on and off—a trade off between phase and amplitude information. The diffraction efficiency is:

$$\eta(s) = \frac{1}{\pi} \sin(\pi s), \quad (13)$$

where s is the on/off rate. Importantly this result indicates that the maximum efficiency a pattern may have is limited to about 32% of the incident amplitude of the diffracting light. If we assume a real valued target pattern this figure doubles to 64% as half the light of these patterns is by default deflected in the opposite direction. Here we are looking for a dithering function (real valued signal) which is dominant over the target mode. For the grating function above we have:

$$U_{mn} = \begin{cases} 1 & \frac{1}{2} a \sin \cos \arg D_{mn} \leq \psi_{mn}^{(N)} / A_{mn} \\ 0 & \text{otherwise,} \end{cases} \quad (14)$$

where $\psi_{mn}^{(N)}$ is a real valued wavefunction normalised to unity peak amplitude and the addition of A_{mn} accounts for the amplitude of light scattered off the device. The $\cos \arg D_{mn}$ may be changed to $|\cos \arg D_{mn}|$ to increase the power dump into the loss channel and remove some periodic noise from a grating (if it was the function used). However, as a

consequence even diffraction orders re-appear. Figure 6 shows some simulated examples of the patterns produced by DMD dithered with the method outlined here. As before, the dithering method works to produce good local approximations of the wavefunction. Figures 6(a)–(c) are representations of the amplitude pattern displayed on the DMD to achieve the local wavefunction approximations shown in (d)–(f). Again, the random noise pattern causes spurious correlations, reducing the fidelity of the resulting mode after spatial filtering. The experimental realisations are shown in (g)–(i). The aberration correction procedure was successful at correcting the point spread function with only minor artefacts present. These artefacts are due to some difficulties with converting the patterns so that they would be accurately displayed on the device and the large block size chosen for the aberration correction procedure [21]. However, the correspondence between each of the scattered wave patterns is excellent, demonstrating that the ability of each method at producing the desired mode amplitudes are virtually identical. This shows that for all intents and purposes the probability distribution of a pixel being on and the amplitude it contributes to the wavefunction are the same regardless of the details of the dithered pattern.

Based on the observations from figure 6 amplitude modulation should be achievable using a pseudo cumulative distribution function (CDF) of the wavefunction due to the devices ability to control probability amplitudes. Consider a real valued wavefunction with an indefinite integral in one dimension approximated by:

$$C_{nj} = \sum_{i=0}^{i=n} \psi_{ij}^{(N)} / A_{mn}$$

with j held constant for each ‘line’ of the other dimension. Discretisation of the resulting distribution function to the number of amplitude levels of the device and transforming back to the amplitude of the wavefunction with a discrete derivative will create a dithered waveform pattern. For example using a central difference:

$$D_{i,j} = [aC_{i+1/2,j}] - [aC_{i-1/2,j}],$$

and for $D_{i,j} > 0$, $U_{i,j} = 1$ and $D_{i,j} \leq 0$, $U_{i,j} = 0$. By default using a pseudo CDF does not result in the maximum diffraction efficiency. A normalisation factor, a , was used to produce images of the ideal amplitude. This number varies depending on periodicity of the carrier grating function and mode. This number was found to be around $a \simeq 1.25 - 1.3$ through trial-and-error.

Figure 7 shows the results of populating an amplitude pattern derived from the cumulative distribution approximated to the whole number. The discrete difference of this pattern produces the dithering pattern shown in (a). Figure 7(b) shows the resulting image plane where the local wavefunction is faithfully produced to a fidelity similar to that seen in figure 6(e). Likewise the experimental result shown in figure 7(c) has excellent correspondence to figure 6(h). The caveat using this method is that despite excellent coverage and uniformity of the DMD it is important to choose the correct scaling of the wave function amplitude to result in

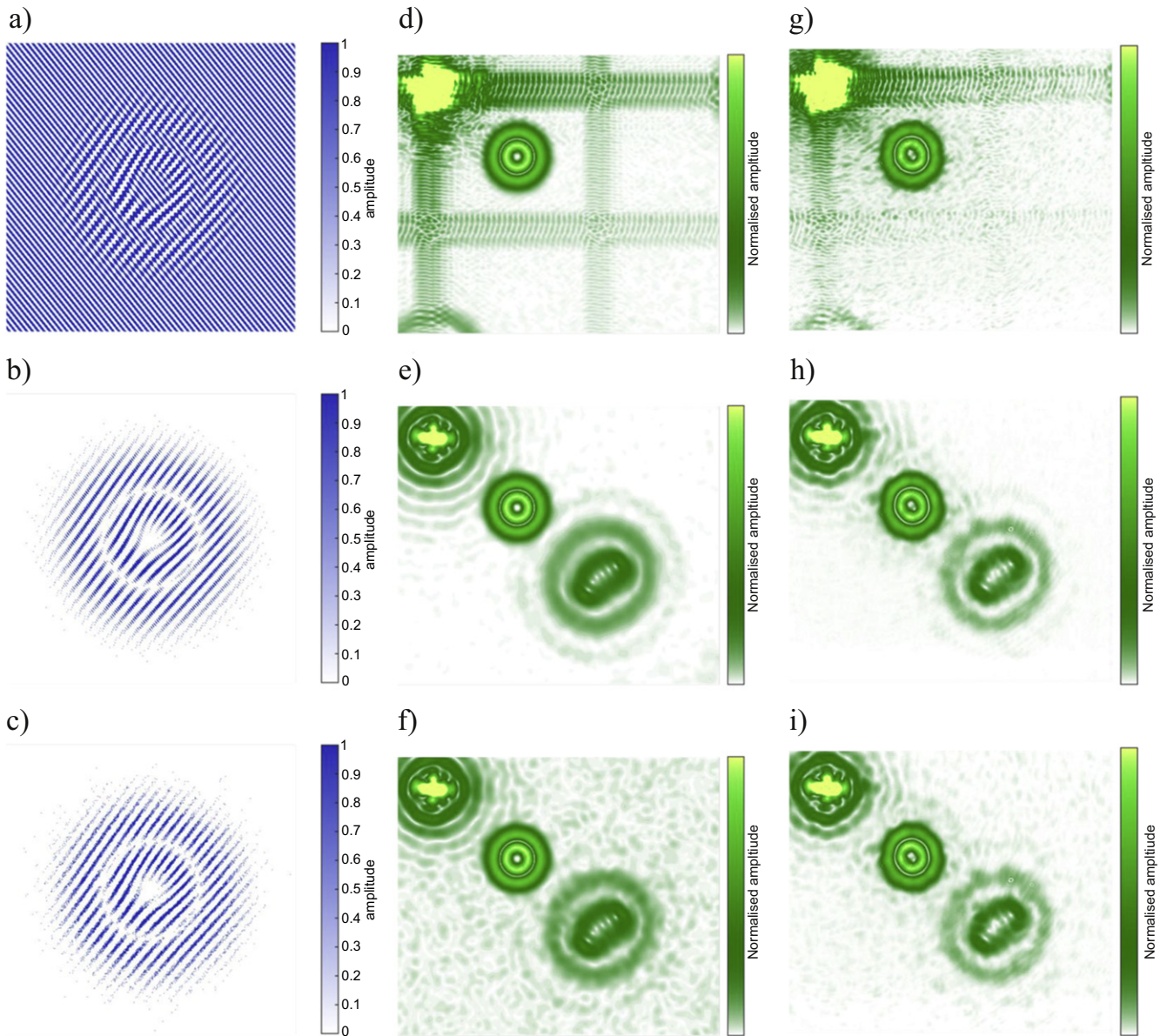


Figure 6. (a)–(c) Amplitude-only holograms. (d)–(f) Simulated diffracted pattern in the conjugate imaging plane for the zero-th and first three orders. (g)–(i) Experimental realisation of the conjugate imaging plane. Holograms for a stationary transverse state of the paraxial wave equation where (a) $f_{mn} = k_x x_m + k_y y_n$ is the grating phase function, (b) same phase function but using the absolute value test criteria to find D_{mn} , (c) $f_{mn} = 2\pi\nu_{mn}$ a white distribution of noise again using the absolute value test criteria.

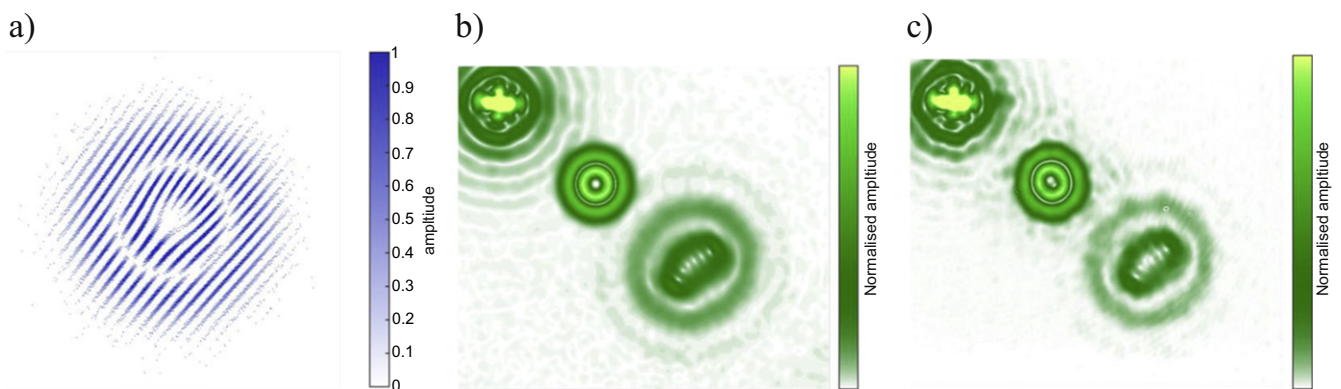


Figure 7. (a) Dithering pattern (based on the derivative of the pseudo-CDF) at the device plane. (b) Simulated waveform in the image plane for a binary level DMD. (c) Experimental realisation of the waveform.

optimum diffraction efficiency. This can be found through simulation of the diffraction pattern. The variation of the normalisation factor with system parameters implies that no simple analytical relationship between its value and the optimum mode diffraction efficiency exists.

5. Discussion of potential experimental variations

It is well known that the diffraction efficiency of a device, especially a phase shifting device such as an SLM is strongly dependent on the correspondence between the controlled parameters and the physical properties of the device, e.g. voltage level and phase. Aberrations of the device are also important for accurate mode generation. For simple spot generation, multiple order diffraction patterns appear. However, for the methods outlined in this article the correspondence of physical device properties and aberrations is significant. The mode pattern we have previously defined was used to generate a diffraction pattern with different voltage to phase level look-up values as parameters. We applied the aberration correction we previously found for the investigation of beam shaping methods. The images displayed in this section were captured by the camera without using pixel intensity linearisation and are therefore not proportional to intensity as it was not needed to demonstrate the properties of the scattered light field.

Figure 8 shows the initial observation of the resulting target pattern for look-up tables over the entire voltage level range, half range, quarter range, and offset (s) by 50 grey levels and for a range (g) of 59 levels. Significant mode artefacts are present, disrupting both the amplitude and phase of the target pattern, finding the ideal look-up results in the highest fidelity reproduction. To investigate the content of these patterns we applied a wedge function phase pattern directly to the initial patterns to separate the spectral components. Using the full range phase pattern results in low fidelity reproduction of the target mode and puts more power in other harmonics. This comports with our previous analysis of diffraction efficiency with phase pitch. The amount of power diverted to our desired target state increases and the other harmonics disappear as we approach the optimised conversion. We also note that the aberration correction required for each set of look-ups changes, which comes as a consequence of the non-uniform phase response with voltage level. We also performed this investigation for the alias pattern filtering method defined in this article. Adding the wedge function here resulted in a separation of harmonics. However, as these harmonics were not initially coincident with the target wavefunction pattern this separation cannot be seen in figure 9. Instead the harmonics moved at harmonic multiples of the initial target wavefunction pattern.

We have several observations based on good agreement between the observed distribution of light and the simulations (where phase could be explicitly determined): (1) The look-up

between device voltage and real phase not only affects the diffraction efficiency of spots, but also the local distribution of amplitude and phase which directly affects mode fidelity. (2) The optimal aberration correction changes as the look-up changes. (3) Different types of target patterns have diverse properties making them more or less sensitive to physical parameters such as actual phase level. (4) No wedge functions have the same diffraction efficiency unless there are no artefacts due to look-up as other harmonics will always overlap and interfere with the target spot pattern.

In our experiments we used a filling of the SLM/DMD such that the tails of our incident Gaussian beam are close to the extremities of our target wavefunction, we therefore had to apply an amplitude correction. Figure 10 shows the resulting scattered light for (a) theoretical target mode amplitudes, (b) the spot pattern when we assumed plane wave illumination, and (c) the spot pattern resulting from assuming the actual incident radiation when calculating the required diffraction pattern. In our case, the plane wave illumination assumption is a poor one as it results in a scattered light pattern which deviates from the ideal beam mode, showing a low central intensity and larger intensity on the outer ring. Applying the amplitude correction adequately removes the variation, yielding a near ideal target pattern.

This section has demonstrated that there is always great potential for any individual beam shaping experiment to demonstrate that one method is worse than another. In these cases great care needs to be exercised when concluding any one method of beam shaping is superior to another. We have indicated here that in many cases deviations in experimental results can be accounted for provided that it is understood how any particular method could be sensitive to experimental parameters such as limitations to the total phase shift of the device or its transmission function.

6. Conclusion

We have discussed methods of applying diffractive optics to the beam mode construction problem in terms of wavefunctions. The discussion of beam shaping methods in these terms leads us to conclude that there is no one 'best' way of producing a beam mode in a single-pass, only that some methods may offer advantages over another for particular experimental configurations. The maximum output amplitude of a shaped mode is equivalent (theoretically) for all valid methods and must therefore only vary due to particular experimental circumstances, such as phase value look-up or aberration. Our experiments accounted for the peculiarities of the device, using look-up tables and aberration correction. Very similar levels of correspondence between the beam shaping methods were obtained. However, in the case where the look-up was poorly known the alias pattern filter used was effective at reproducing the target mode pattern provided the aberration correction was optimised for that particular look-up table.

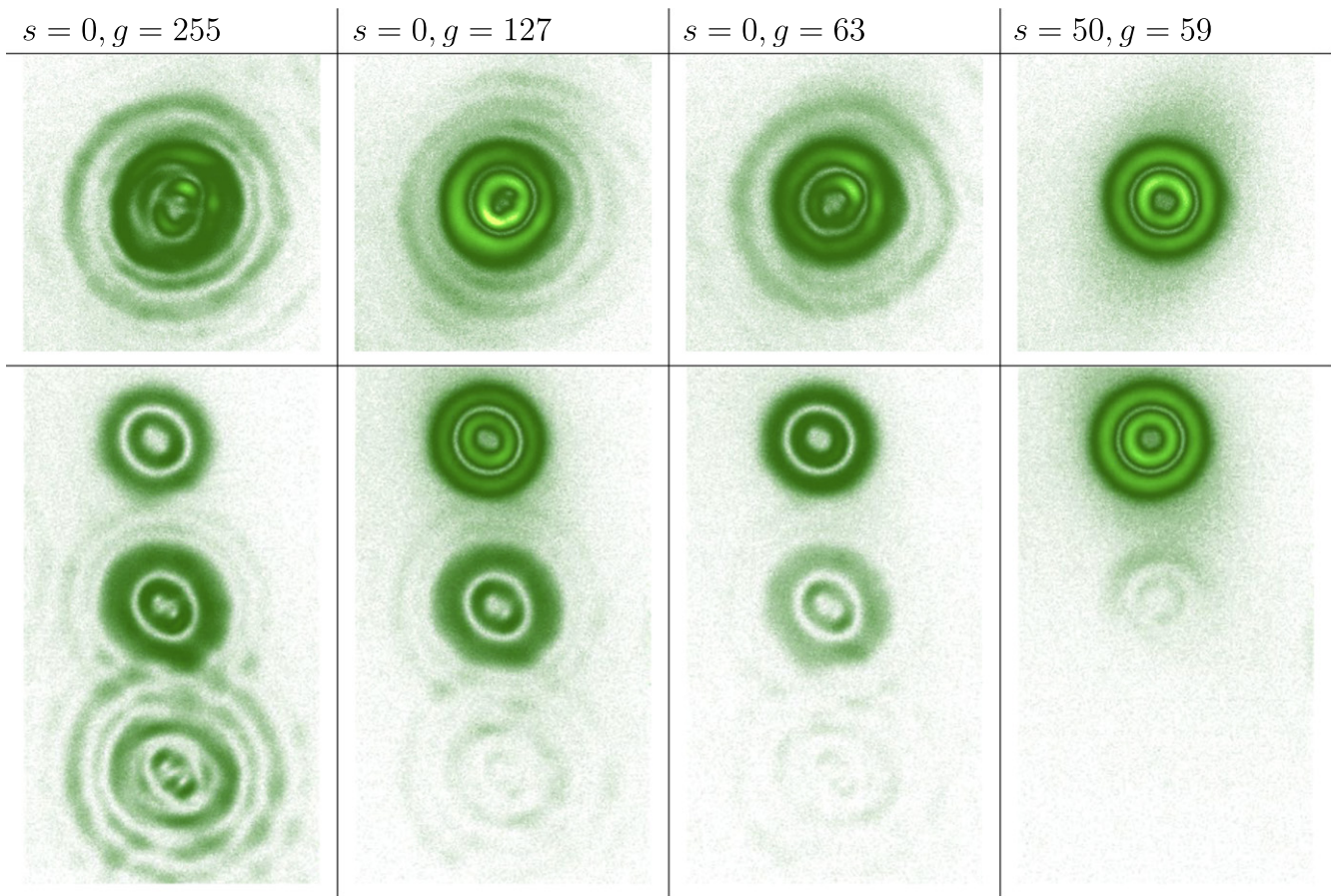


Figure 8. The diffracted spot pattern resulting from different look-up values. s and g correspond to the look-up equation (3). Mode artefacts may be separated into harmonics through application of wedge functions. The optimised look-up used in our experiment result in only small harmonics.

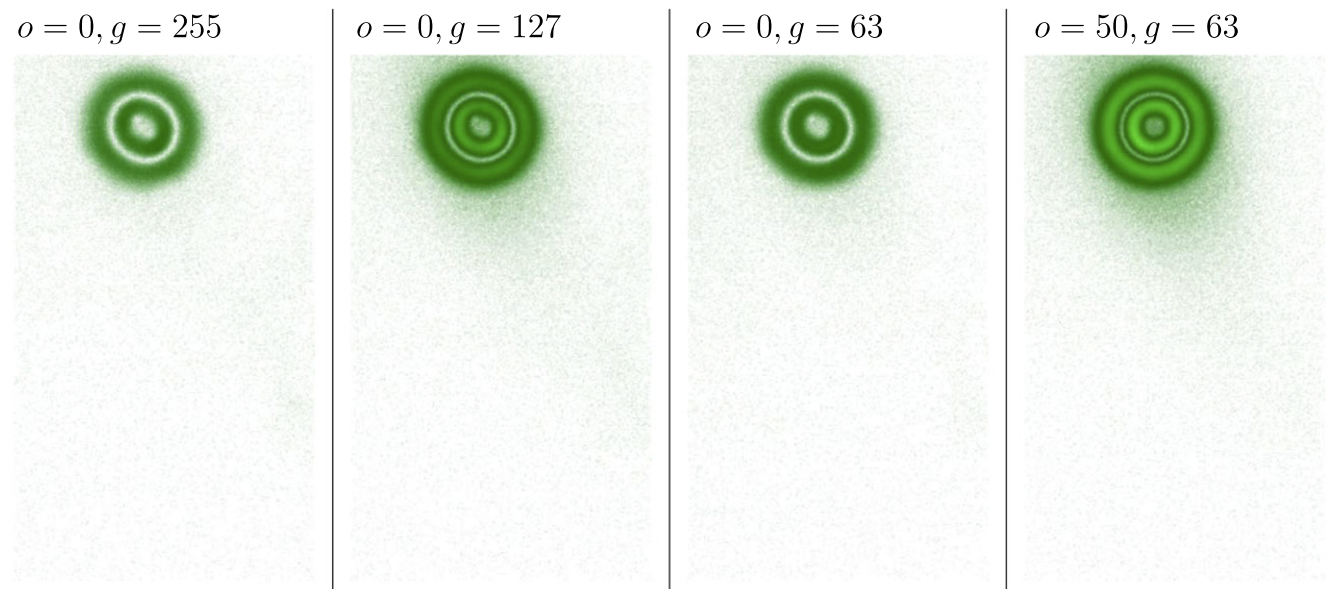


Figure 9. The diffracted spot pattern resulting from different look-up values for the alias filter pattern method. In this case the application of wedge function has no local effect on the distribution of light. Instead these harmonics were already present at other points in space and thus not contaminating the target region.

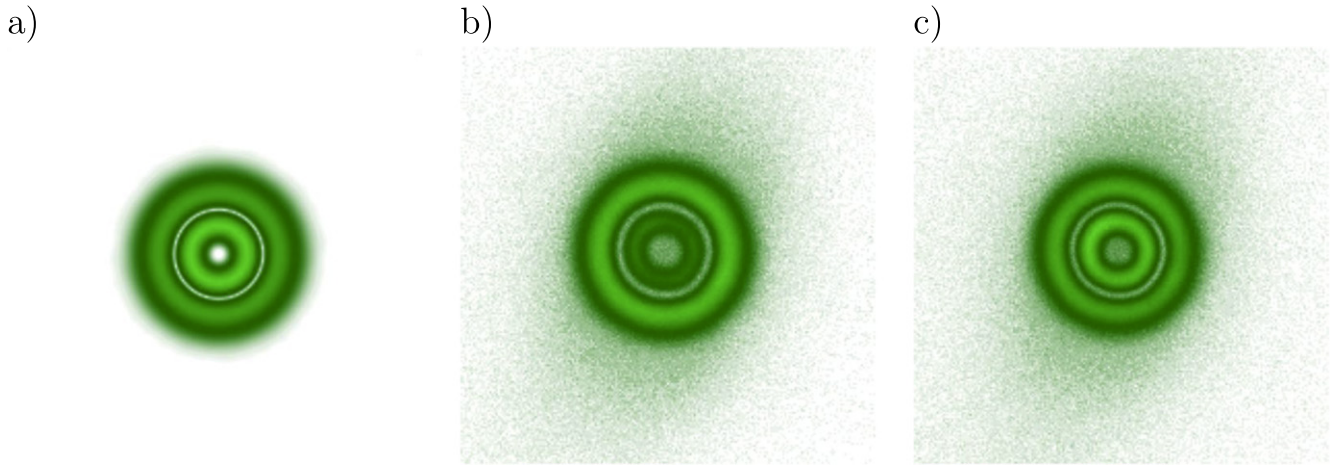


Figure 10. (a) Theoretical amplitude distribution of the target wavefunction. (b) Detected scattered light assuming plane wave illumination. (c) Light scattered from an amplitude corrected pattern.

Appendix. Derivation of equation (10)

Consider the mode overlap:

$$\eta(c) = \frac{1}{N} \sum_{n=1, m=1}^N \exp\left(i(o-c)(-1)^n(-1)^m \frac{\pi}{2}\right) \quad (\text{A.1})$$

and for an even number of elements we find:

$$\eta(c) = \frac{1}{N} \sum_{n=1, k=1}^{N/2} \exp\left(i(o-c)(-1)^n(-1)^{2k} \frac{\pi}{2}\right) + \exp\left(i(o-c)(-1)^n(-1)^{2k-1} \frac{\pi}{2}\right) \quad (\text{A.2})$$

$$= \frac{1}{N} \sum_{n=1, k=1}^{N/2} 2 \cos\left((o-c)(-1)^n(-1)^{2k} \frac{\pi}{2}\right) \quad (\text{A.3})$$

and as the cosine function is even our choice of n is irrelevant and so obtain cancelations which result in:

$$\eta(c) = \cos(o-c) \frac{\pi}{2}. \quad (\text{A.4})$$

Further, the concept of order has no real particular meaning with regard to the maximum frequency of the device as all orders are aliased to the same frequency. We can arbitrarily pick any o which will always result in effectively the same inverse function for a given input. We could for example pick $o = 1$ simply to be consistent with the previously defined case:

$$\eta(c) = \cos(1-c) \frac{\pi}{2}. \quad (\text{A.5})$$

Funding

This work is supported by Australian Research Council Discovery Grant DP140100753.

References

- [1] Fürhapter S, Jesacher A, Bernet S and Ritsch-Marte M 2005 Spiral phase contrast imaging in microscopy *Opt. Express* **13** 689–94
- [2] Fickler R, Lapkiewicz R, Plick W N, Krenn M, Schaeff C, Ramelow S and Zeilinger A 2012 Quantum entanglement of high angular momenta *Science* **338** 640–3
- [3] Wang J *et al* 2012 Terabit free-space data transmission employing orbital angular momentum multiplexing *Nat. Photon.* **6** 488–96
- [4] Li L, Gattass R R, Gershgoren E, Hwang H and Fourkas J T 2009 Achieving $\lambda/20$ resolution by one-color initiation and deactivation of polymerization *Science* **324** 910–3
- [5] Woerdemann M, Alpmann C, Esseling M and Denz C 2013 Advanced optical trapping by complex beam shaping *Laser Photonics Rev.* **7** 839–54
- [6] Kozma A and Kelly D L 1965 Spatial filtering for detection of signals submerged in noise *Appl. Opt.* **4** 387–92
- [7] Kirk J P and Jones A L 1971 Phase-only complex-valued spatial filter *J. Opt. Soc. Am.* **61** 1023–8
- [8] Davis J A, Cottrell D M, Campos J, Yzuel M J and Moreno I 1999 Encoding amplitude information onto phase-only filters *Appl. Opt.* **38** 5004–13
- [9] Bagnoud V and Zuegel J D 2004 Independent phase and amplitude control of a laser beam by use of a single-phase-only spatial light modulator *Opt. Lett.* **29** 295–7
- [10] Arizón V, Ruiz U, Carrada R and González L A 2007 Pixelated phase computer holograms for the accurate encoding of scalar complex fields *J. Opt. Soc. Am. A* **24** 3500–7
- [11] Matsumoto N, Ando T, Inoue T, Ohtake Y, Fukuchi N and Hara T 2008 Generation of high-quality higher-order laguerre-gaussian beams using liquid-crystal-on-silicon spatial light modulators *J. Opt. Soc. Am. A* **25** 1642–51
- [12] Jesacher A, Maurer C, Schwaighofer A, Bernet S and Ritsch-Marte M 2008 Near-perfect hologram reconstruction with a spatial light modulator *Opt. Express* **16** 2597–603
- [13] van Putten E G, Vellekoop I M and Mosk A P 2008 Spatial amplitude and phase modulation using commercial twisted nematic LCDs *Appl. Opt.* **47** 2076–81
- [14] Wong D W K and Chen G 2008 Redistribution of the zero order by the use of a phase checkerboard pattern in computer generated holograms *Appl. Opt.* **47** 602–10

- [15] Liang J *et al* 2010 High-precision laser beam shaping using a binary-amplitude spatial light modulator *Appl. Opt.* **49** 1323–30
- [16] Goorden S A, Bertolotti J and Mosk A P 2014 Superpixel-based spatial amplitude and phase modulation using a digital micromirror device *Opt. Express* **22** 17999–8009
- [17] Schuchman L 1964 Dither signals and their effect on quantization noise *IEEE Trans. Commun. Technol.* **12** 162–5
- [18] Tay J W, Taylor M A and Bowen W P 2009 Sagnac-interferometer-based characterization of spatial light modulators *Appl. Opt.* **48** 2236–42
- [19] Persson M, Engström D and Goksör M 2012 Reducing the effect of pixel crosstalk in phase only spatial light modulators *Opt. Exp.* **20** 22334–43
- [20] Lingel C, Haist T and Osten W 2013 Optimizing the diffraction efficiency of SLM-based holography with respect to the fringing field effect *Appl. Opt.* **52** 6877–83
- [21] Čižmár T, Mazilu M and Dholakia K 2010 *In situ* wavefront correction and its application to micromanipulation *Nat. Photon.* **4** 388–94
- [22] Debevec P E and Malik J 1997 Recovering high dynamic range radiance maps from photographs *Proc. 24th Annu. Conf. on Computer Graphics and Interactive Techniques* pp 369–78
- [23] Brown B R and Lohmann A W 1966 Complex spatial filtering with binary masks *Appl. Opt.* **5** 967–9
- [24] Porter A B 1906 On the diffraction theory of microscopic vision *Philosophical Magazine* vol 11 (London: Taylor and Francis) pp 154–66 ch 12